Desalination and Water Treatment
www.deswater.com

doi:10.5004/dwt.2016.0160

59 (2017) 272–279
January

MCM-41 impregnated with various weight percentages of zeolite X precursors for tetracycline removal

Minmin Liu[a,b], Li-an Hou[b], Qi Li[b], Yufei Shangguan[b], Xiaojun Hu[a]*, Shuili Yu[b]*

[a]*School of Chemical and Environmental Engineering, Shanghai Institute of Technology, 500 Haiquan Road, Shanghai, China, email: lmm@sit.edu.cn (Minmin Liu), Tel./Fax +86 13045681913, email: hxjsit@sina.com (X. Hu)*
[b]*State Key Laboratory of Pollution Control and Resource Reuse, School of Environmental Science and Engineering, Tongji University, 1239 Siping Road, Shanghai 200092, China, email: houli_an@sina.com (L. Hou), liqitongji@sina.com (Q. Li), shangguan940807@163.com (Y. Shangguan) ysl@tongji.edu.cn (S. Yu)*

Received 5 February 2016; Accepted 12 June 2016

ABSTRACT

The new adsorbents ((n% of zeolite X precursor) X-MCM-41) were prepared to remove tetracycline (TC) from water. The TC adsorption capacities of (n)X-MCM-41 increased as the weight percentages of zeolite X precursor increased. Compared with other (n)X-MCM-41 adsorbents, the TC adsorption capacity of (3)X-MCM-41 was maximum and reached 503.7 mg g^{-1}. The TC adsorption capacity of (n) X-MCM-41 in acidic and neutral conditions was more than that in alkaline condition. The Langmuir isotherm models described the TC adsorption isotherms of (n)X-MCM-41 very well. The adsorption kinetics behavior of (n)X-MCM-41 was well described by both pseudo-second order and the intra-particle diffusion models. The TC adsorption behavior of (n)X-MCM-41 was ion exchange reaction and electrostatic adsorption.

Keywords: MCM-41; Tetracycline; Isotherms; Mesoporous sieve; Zeolite

1. Introduction

The TC antibiotics are harmful to human health. The high TC application in aquatic environments could increase the number of antibiotics resistance bacteria among microbial populations [1]. Thus, it is necessary to develop efficient methods for TC removal from water. Many methods are available for TC removal such as advanced oxidation and biodegradation processes [2–4]. Especially, the adsorption method is practical and effective for TC removal from water in situ.

There were many adsorbents studied for TC removal from water such as activated carbon, clay minerals, multi-walled carbon nanotubes, modified nanoscale zero valent iron, hydrous manganese oxide aluminum and iron hydrous oxides [5–7]. The TC was removed by adsorbents from water through different mechanisms such as surface complexation and electrostatic adsorption. Among these adsorbents, the mesoporous materials with ordered pore structure and large surface area were suitable for water purification [8]. For example, MCM-41 was applied to remove nitrobenzene, phenol, o-chlorophenol and divalent metal cations from water [9–12]. Modified mesoporous silica was good adsorbent for heavy metal ions removal from aqueous solutions [13]. In addition, MCM-41 materials were modified to adsorb anionic dyes and mercury [14,15]. The adsorption capacities of the heavy metal ions by mesoporous adsorbents were enhanced through the combination of MCM-41 with the cation exchange capacity of the zeolite [16].

In the study, the novel (n)X-MCM-41 adsorbents were prepared through the impregnation of various weight percentages of zeolite X precursors into MCM-41. The TC adsorption process of (n)X-MCM-41 was described by the adsorption isotherms and kinetics models. The effects of various parameters on the TC adsorption were studied and the mechanisms were proposed.

*Corresponding author.

2. Materials and methods

2.1. Materials and chemicals

Hydrochloride salt of tetracycline (MW: 480.90) was purchased from Sigma Co. Cetyltrimethylammonium bromide (CTAB) and tetraethyl orthosilicate (TEOS) were supplied by Aldrich (U.K.). Sodium silicate, sodium aluminate, sodium hydroxide, and hydrochloric acid were provided by Fisher Scientific.

2.2. Synthesis procedures

The chemicals with the molar ratio of Na_2O: Al_2O_3: SiO_2: H_2O being 7.15: 1: 2.2: 122 were mixed in the solution. Then the mixture was heated to the boiling state and stirred for 1 h. Then the mixed solution was aged at 298 K in a static state for 24 h to form the zeolite X precursors.

The chemicals were mixed in the solution with the molar ratio of (SiO_2 + Al_2O_3):NaOH:C_{16}TMABr:H_2O being 1:0.24:0.12:100. Especially, the molar ratio of SiO_2:Al_2O_3 was 20:1. Then various weight percentages of zeolite X precursors (1, 2, 3 and 4%) were added to the solution. Then the pH of the solution was adjusted to 10.5 with hydrochloric acid and the white gel was formed under the condition of continuous stirring for 1 h. The gel was transferred into a 200 mL Teflon-lined stainless autoclave. Subsequently, it was crystallized at 378 K for 48 h. After crystallization, the autoclave was cooled to room temperature naturally. Then the white gel was calcined in air at 823 K for 4 h. Finally, the white powder (n)X-MCM-41 was obtained. The n represents the weight percentage of zeolite X precursors. The values of n were 1, 2, 3 and 4.

2.3. Characterization and analysis

The small-angle X-ray scattering (SAXS) measurements of samples were carried out with a Philips X' pert powder diffractometer system with Cu-Kα (λ = 1.541 A) radiation. The Brunauer-Emmett-Teller (BET) specific surface areas of adsorbents were examined by the N_2 sorption-desorption isotherms method. The contents of the Si, Al and Na in the sample was determined using energy dispersive X-ray fluorescence (XRF) (Oxford ED2000). The ATI Mattson FTIR spectrophotometer was used to detect the infrared spectra of all samples. The Transmission electron microscopy (TEM) images were taken by the H-8100 transmission electron microscopy at 200 kV. The TC concentration was determined by high performance liquid chromatography (Agilent, USA). Column: Agilent HC-C18, 5 μm, 4.6 × 250 mm^2; the mobile phase: the mixture of 0.01 M disodium hydrogen phosphate-acetonitrile; flow rate: 1 mL min^{-1} and the detector: UV at 355 nm. The pH_{ZPC} values of samples were determined by the batch equilibrium experiments [17].

2.4. Adsorption batch experiments

The 1g L^{-1} adsorbent was added to the solutions of various TC concentrations. The pH of TC solutions was adjusted by 0.01 M NaOH or HCl solution. All of the vials were stirred in the shaker at 298 K for 48 h in the dark. At selected time intervals, the 1 mL of the solution was taken out and filtered through the 0.45 μm membrane filter. Then the TC concentration was measured by HPLC. During the period, there was no apparent TC degradation in the solution without adsorbents.

2.5. Adsorption isotherms

The equation of Freundlich model is presented as follows [18]:

$$\log(q_e) = \log k_f + 1/n \log(c_e) \quad (1)$$

where k_f and $1/n$ are Freundlich constants which refers to adsorption capacity and adsorption intensity, respectively [19].

The Langmuir model is shown as the following equation [18]:

$$\frac{1}{q_e} = \frac{1}{q_{\max} K_L} \bullet \frac{1}{C_e} + \frac{1}{q_{\max}} \quad (2)$$

where q_e represents the amount of TC adsorbed on adsorbents at equilibrium. C_e is the TC equilibrium concentration. q_{max} is the TC adsorption capacity. The parameter K_L is the Langmuir adsorption equilibrium constant.

The Dubnin-Radushkevich (D-R) isotherm can also describe the TC adsorption process. The equation is as follows:

$$\ln q_e = \ln q_m - K\varepsilon^2 \quad (3)$$

where K is the constant which refers to the mean free energy of TC adsorption process. The q_m is the theoretical saturation capacity of TC (mg g^{-1}), and ε is the Polanyi potential ($\varepsilon = RT\ln(1 + \frac{1}{C_e})$). The D-R constant can supply the valuable information on the mean energy of adsorption by the following equation:

$$E = (2K)^{-1/2}$$

2.6. Adsorption kinetics

The equations of adsorption kinetics models are presented as follows [19]:

The pseudo-first-order model $\ln(q_e - q(t_i)) = \ln q_e - k_1 t$ (4)

The pseudo-second-order model $\frac{t}{q(t_i)} = \frac{1}{k_2 q_e^2} + \frac{t}{q_e}$ (5)

The intra-particle diffusion model $q(t_i) = k_3 t^{1/2} + C$ (6)

where k_1 (min^{-1}), k_2 (g mg^{-1} min^{-1}) and k_3 (mg g^{-1} $min^{1/2}$) are the adsorption rate constants of pseudo-first-order equation, pseudo-second-order equation and the intra-particle diffusion model, respectively. The C is related with the thickness of the boundary layer. The q_e and $q(t_i)$ (mg g^{-1}) are the amount of TC adsorbed on (n)X-MCM-41 at equilibrium and time t_i, respectively.

3. Results and discussion

3.1. Samples characterizations

3.1.1. X-ray diffraction

As shown in Fig. 1A, (n = 1, 2, 3) X-MCM-41 exhibited the typical diffraction peaks except (4)X-MCM-41 in the low 2θ region. It demonstrated that the (n = 1, 2, 3) X-MCM-41 might have the uniform pores. However, the (4) X-MCM-41 did not have the diffraction peak. It indicated the (4) X-MCM-41 did not have pores structure due to the overload of zeolite X. Fig. 1B presents the diffraction peak of zeolite X was not detected in the wide angle XRD patterns of (n)X-MCM-41.

3.1.2. N_2 adsorption-desorption isotherm and element content

From Fig. 2, the N_2 adsorption-desorption isotherms for (n)X-MCM-41 display hysteresis loop which is contributed to slit-shaped pores [20]. The addition of zeolite X precursor to the synthesis gel could cause defects in the (n) X-MCM-41 [20].

As shown in Table 1, the Si/Al atom mole ratios of the solid samples were higher than those of the gel. It indicated Al atoms were incorporated into the structure of MCM-41. If an Al atom incorporation makes the [AlO_4] unit instead of [SiO_4] unit, a cation will be needed to make charge balance. Thus, the ideal Na/Al mole ratio is one [21]. The Na/Al mole ratio of the sample (3)X-MCM-41 was about 1. For other samples, the additional Na cations might be bonded to the surface.

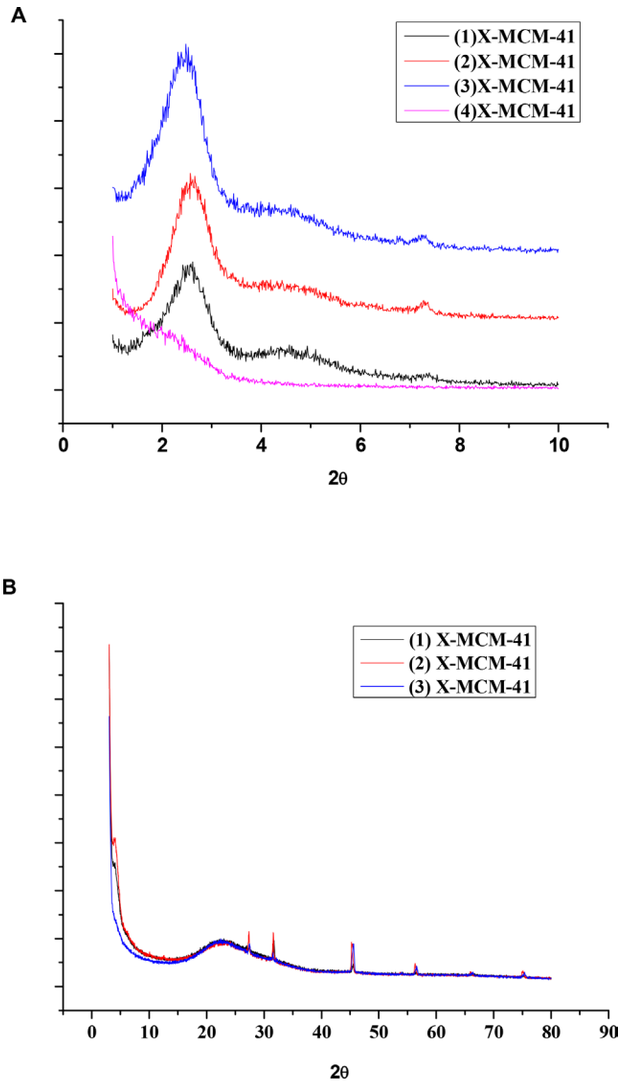

Fig. 1. (A) The small angle XRD; (B) the wide angle XRD of (n) X-MCM-41.

3.1.3. Fourier Transform Infrared (FTIR) spectroscopy

From Fig. 3A, the vibrational bands at 465 cm^{-1} and 1087 cm^{-1} are assigned to the structural characteristics of silica framework similar with MCM-41 [22]. The bands at 1634 cm^{-1} and 3445 cm^{-1} are attributed to water molecules in the samples [22]. It indicates the samples are hydrophilic. The vibration band of 550 cm^{-1} is similar with that of zeolite X and as the amount of zeolite X increases, the vibration band of 550 cm^{-1} was increased. It illustrated zeolite X structure formed in the framework of samples [23].

TC contains three functional groups such as tricarbonylamide, phenolic diketone, and dimethylamine [24]. From Fig. 3B, the spectrum between 1200 and 1750 cm^{-1} denotes

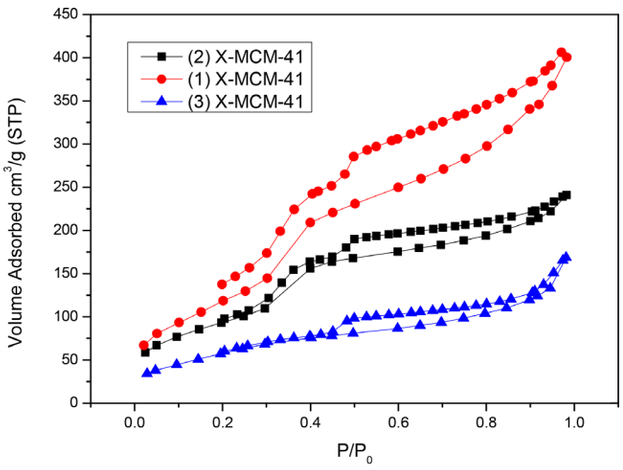

Fig. 2. N_2 adsorption-desorption isotherms.

Table 1
Elements atom mole ratios of (n)X-MCM-41

Sample	Gel Si/Al mole ratio	Si/Al mole ratio from XRF	Gel Na/Al mole ratio	Na/Al mole ratio from XRF
(1)X-MCM-41	9.85	12.32	2.63	1.56
(2)X-MCM-41	9.74	11.84	2.41	1.35
(3)X-MCM-41	9.56	10.95	2.18	0.98

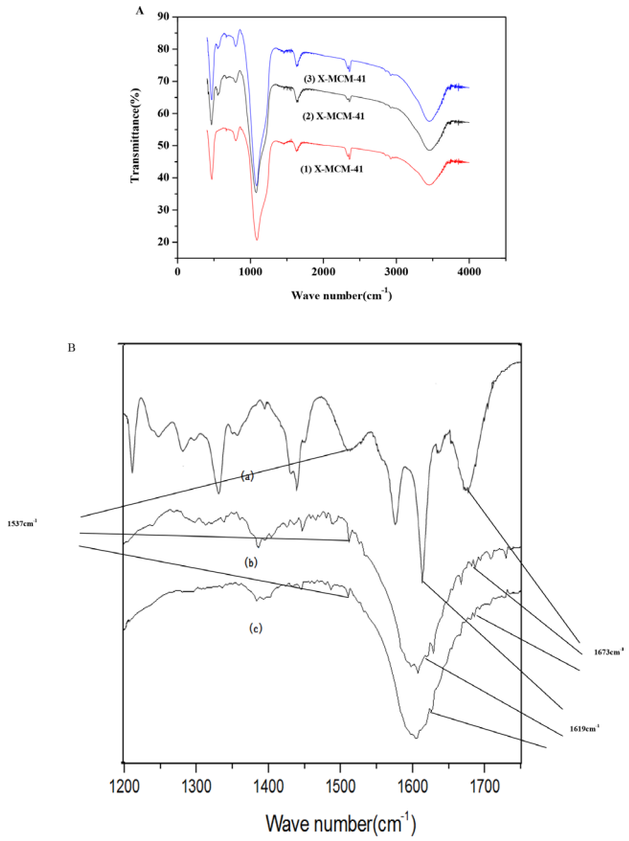

Fig. 3. (A) FTIR; (B) FTIR spectra of TC (a), (1)X-MCM-41 after TC adsorption (b), and (3)X-MCM-41 after TC adsorption (c).

the most characteristic region of the TC spectrum. The bands at 1537 and 1673 cm^{-1} were attributed to the amino and carbonyl groups of TC, respectively [25]. The bands at 1619 and 1586 cm^{-1} were assigned to the carbonyl groups of TC. The bands at 1537 and 1673 cm^{-1} of (1)X-MCM-41 and (3)X-MCM-41 almost disappeared. It demonstrated that the carbonyl and amino groups of TC reacted with the adsorbents. From Fig. 5, the pH_{zpc} of (n)X-MCM-41 was below pH 7. Therefore, the surface of (n)X-MCM-41 was negatively charged at pH 7. Thus, the (n)X-MCM-41 could react with the positive charged nitrogen of TC.

3.1.4. The TEM image

The Fig.4 shows the TEM image of the (3)X-MCM-41. It presents that the sample has the structure of pores after impregnation with zeolite X precursor.

3.1.5. The pH_{zpc}

From Fig.5, the pH_{zpc} of (n)X-MCM-41 was decreased from 2.5 for (1)X-MCM-41 to 1 for (3)X-MCM-41. If the pH of the solution is lower than the pH_{zpc}, the adsorbent surface will be positively charged. If the pH is above pH_{zpc}, the surface of the sample will be negatively charged. It illustrated the negative charge of adsorbent surface was increased as the content of zeolite X precursors increased. Since the

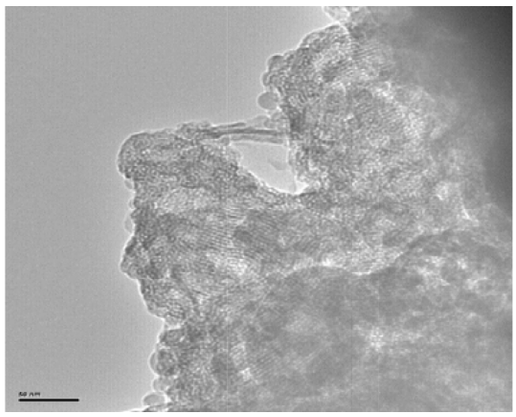

Fig. 4. TEM image of (3)X-MCM-41.

(n)X-MCM-41 reacted with the positive charged nitrogen of TC, the TC adsorption efficiency of (n)X-MCM-41 was enhanced as the content of zeolite X precursors increased due to the electrostatic adsorption.

3.2. Effect of pH

From Fig. 6A, the cation (TCH^{3+}), zwitterion (TCH_2^0) and anion (TCH^- or TC^{2-}) are formed by the protonation-deprotonation transition of functional groups of TC due to the pH variation [27]. Thus, the pH of TC solution is one of the most important parameters affecting the TC adsorption on (n)X-MCM-41. From Fig. 6B, the TC adsorption capacity of (3)X-MCM-41 was 457 mg g^{-1} at pH 3. The adsorption capacity of TC was increased to 492 mg g^{-1} as the pH increased to 7. The adsorption capacity of TC was decreased to 316.2 mg g^{-1} at pH 8.0. Therefore, the adsorption of TC on (3)X-MCM-41 was efficient in the acidic or neutral solution.

As shown in Fig. 5, as pH is above the pH_{zpc} of (n)X-MCM-41, TCH^{3+} and TCH_2^0 are the predominant TC species at pH between 2 and 7 and could be adsorbed on negatively charged surface of (n)X-MCM-41. When pH is above 7.7, TCH^- and TC^{2-} are the main TC species and could not be adsorbed on the adsorbent due to the electrostatic repulsion. From Fig. 6C, after the zeolite X precursors were introduced into the framework of MCM-41, the unsaturated negative charge surface environment was generated. The ion exchange reaction between (n)X-MCM-41 and TCH_3^+ can be expressed by the following equation.

$$(n = 1, 2, 3)X\text{-}MCM\text{-}41\text{-}Na^+ + TCH_3^+ \leftrightarrow (n = 1, 2, 3)X\text{-}MCM\text{-}41\text{-}TCH_3 + Na^+$$

As pH is below 3.3, TCH_3^+ is the main TC species and the surface of (n)X-MCM-41 is negatively charged. The TC was removed by (n)X-MCM-41 from water through ion exchange reaction and electrostatic adsorption.

3.3. Adsorption isotherms

The adsorption isotherms of (n)X-MCM-41 were described by Langmuir, Freundlich and D-R isotherms

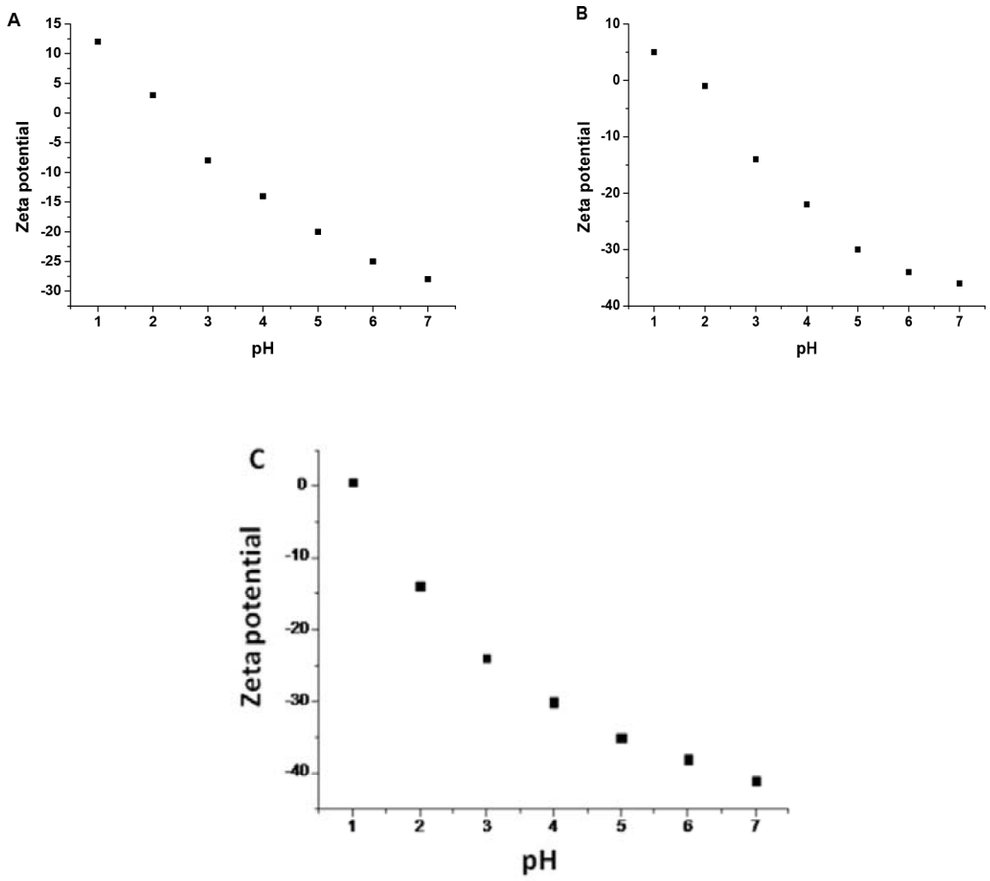

Fig. 5. pH_{zpc} plots of adsorbents (A) (1)X-MCM-41; (B) (2)X-MCM-41; (C) (3)X-MCM-41.

models. From Table 2 and Fig. 7, the correlation coefficients R^2 of Langmuir isotherms model were much closer to 1. It indicated the TC adsorption behavior of (n)X-MCM-41 followed monolayer adsorption. In addition, the TC adsorption capacities of (n)X-MCM-41 were increased as the content of zeolite X precursors increased. The maximum TC adsorption capacity of (3)X-MCM-41 was 503.7 mg g^{-1}. As shown in Table 3, the (3)X-MCM-41 was the effective adsorbent for TC removal compared with other adsorbents.

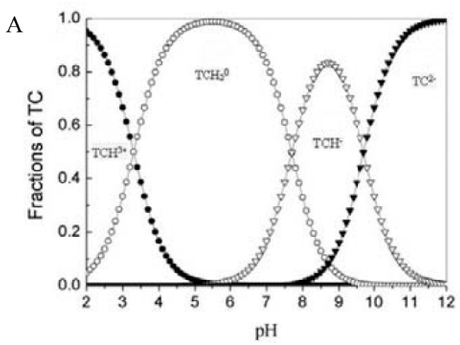

Fig. 6A. The fraction of cationic, neutral and anionic forms of TC at different pHs.

3.4. Adsorption kinetics

From Fig. 8 and Table 4, the TC adsorption process of (n) X-MCM-41 fitted the pseudo-second order kinetics model. It indicated the TC adsorption kinetics was linearly related with the square of the number of adsorption sites [26]. It also suggested chemical adsorption was the rate controlling process of TC adsorption.

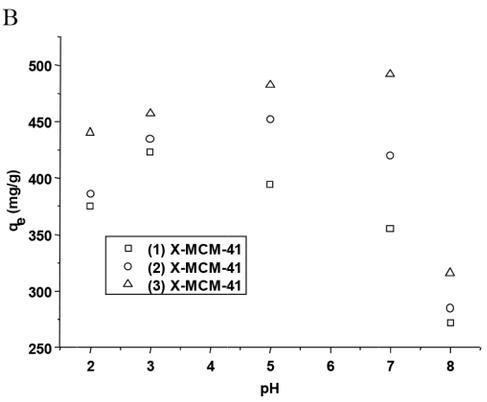

Fig. 6B. The TC adsorption efficiency by (n)X-MCM-41 at various pHs (the initial concentration of TC, 200mg L^{-1}; temperature, 298 K).

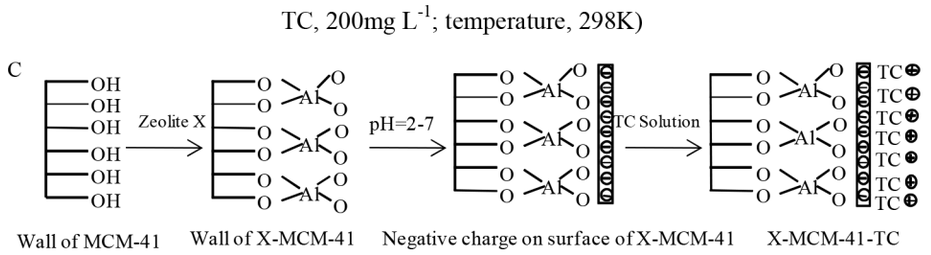

Fig. 6C. The proposed mechanism of zeolite X impregnated into MCM-41 and TC adsorption by (n) X-MCM-41.

Table 2
The parameters of isotherm models of TC adsorption on (n)X-MCM-41

Adsorbents	Freundlich			Langmuir		
	k_f	n	R^2	q_{max} (mg g^{-1})	K_L (L mg^{-1})	R^2
Zeolite X	568.2 ± 1.2	15.64 ± 0.06	0.836	384.6 ± 0.2	1.32 ± 0.15	0.934
(1)X-MCM-41	452.1 ± 1.5	1.25 ± 0.21	0.82	414.5 ± 1.6	0.57 ± 0.05	0.954
(2)X-MCM-41	540.2 ± 1.3	1.75 ± 0.31	0.85	468.3 ± 2.2	0.68 ± 0.07	0.969
(3)X-MCM-41	563.8 ± 0.6	1.89 ± 0.25	0.89	503.7 ± 3.1	0.73 ± 0.06	0.981

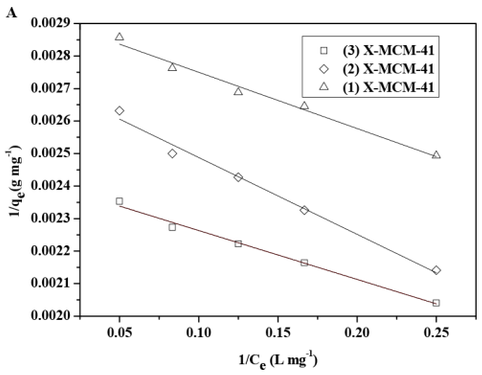

Fig. 7. Langmuir isotherms model of TC adsorption on (n) X-MCM-41.

Table 3
Maximum TC adsorption capacity (q_m) of various adsorbents

Adsorbents	q_m (mg g^{-1})	Refs.
montmorillonite	283	[24]
Multi-walled carbon nanotubes	269.54	[25]
Magnetic microspheres	365	[26]
Graphene oxide	313	[27]
Smectite	462	[28]
cryogels	108	[29]
organo-montmorillonites	434	[30]
(3)X-MCM-41	503.7	This study

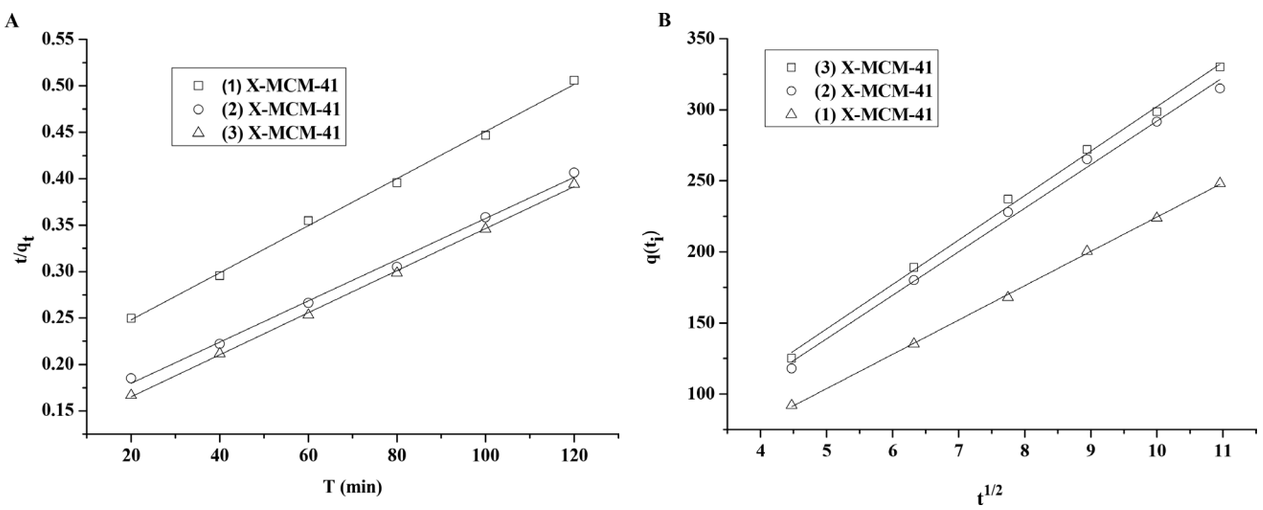

Fig.8 (A) The plots of the pseudo-second order and (B) the intra-particle diffusion kinetics models for (n) X-MCM-41

Table 4
The kinetics and intra-particle diffusion model of TC adsorption onto (n) X-MCM-41

Kinetic models	Parameters	Adsorbents		
		(1)X-MCM-41	(2)X-MCM-41	(3)X-MCM-41
Pseudo-second-order parameters	q_e(mg g^{-1})	434	506	535
	K_2(min^{-1})	0.058	0.0468	0.0457
	R^2	0.997	0.996	0.999
Intra-particle diffusion parameters	K_3 (mg g^{-1} min$^{-1/2}$)	21.96	27.56	28.15
	C	2.71	3.41	7.61
	R^2	0.998	0.996	0.992

From Fig. 8B, the values of K_3 were obtained from the plots of q_t vs t. As shown in Table 3, as the content of zeolite X increased, the values of K_3 were increased. It suggested the adsorption efficiency of (n)X-MCM-41 was increased as the content of zeolite X increased. The C value of (3)X-MCM-41 was largest. It indicated the boundary layer made the greatest influence on the TC adsorption by (3)X-MCM-41. In contrast, the *C* value of (1)X-MCM-41 was smallest. It indicated the TC adsorption efficiency of (1)X-MCM-41 was mainly controlled by intra-particle diffusion.

4. Conclusions

The TC adsorption efficiency of the modified MCM-41 adsorbents was studied. The TC adsorption capacity of (n)X-MCM-41 was enhanced as the weight percentage of zeolite X precursors increased from 1 to 3% because the ion exchange capacity and surface negative charge of (n) X-MCM-41 increased. The maximum TC adsorption capacities of (1)X-MCM-41, (2)X-MCM-41 and (3)X-MCM-41 were 414.5, 468.3 and 503.7 mg g^{-1}, respectively. The TC adsorption capacity of (n)X-MCM-41 in acidic and neutral conditions was more than that in alkaline condition. The TC was removed by (n)X-MCM-41 through ion exchange reaction and electrostatic adsorption.

Acknowledgments

This work was supported by the Program of Shanghai Institute of Technology (YJ2015-33), the National Natural Science Foundation of China (21277093), Program for New Century Excellent Talents in University (NCET-13-0910), National Natural Science Foundation of China (21007048), Key Projects in the National Science & Technology Pillar Program during the Twelfth Five-year Plan Period (2012BAJ25B06) and Twelfth Five-year Plan Period of Major Science and Technology Program for Water Pollution Control and Treatment (2012ZX07403-001).

References

[1] B. Han, F. Zhang, Z. Feng, A designed Mn_2O_3/MCM-41 nanoporous composite for methylene blue and rhodamine B removal with high efficiency, Ceram. Int., 40 (2014) 8093–8101.
[2] S.A. Idris, C.M. Davidson, C. McManamon, Large pore diameter MCM-41 and its application for lead removal from aqueous media, J. Hazard. Mater., 185 (2011) 898–904.
[3] M.M. Liu, D. An, L.A. Hou, S.L. Yu, Y.Q. Zhu, Zero valent iron particles impregnated zeolite X composites for adsorption of tetracycline in aquatic environment, RSC Adv. 5 (2015) 103480–103487.
[4] N. Wu, W. Zhang, B. Li, Nickel nanoparticles highly dispersed with an ordered distribution in MCM-41 matrix as an efficient catalyst for hydrodechlorination of chlorobenzene, Micropor. Mesopor. Mater., 185 (2014) 130–136.
[5] I. Ursachi, A. Vasile, A. Ianculescu, Ultrasonic-assisted synthesis and magnetic studies of iron oxide/MCM-41 nanocomposite, Mater. Chem. Phys., 130 (2011) 1251–1259.
[6] V. Elías, E. Sabre, E. Winkler, Chromium and titanium/chromium-containing MCM-41 mesoporous silicates as promising catalysts for the photobleaching of azo dyes in aqueous suspensions. a multitechnique investigation, Micropor. Mesopor. Mater., 163 (2012) 185–195.
[7] P.A. Mangrulkar, S.P. Kamble, J. Meshram, S.S. Rayalu, Adsorption of phenol and o-chlorophenol by mesoporous MCM-41, J. Hazard. Mater., 160 (2008) 414–421.
[8] K.A. Northcott, K. Miyakawa, S. Oshima, The adsorption of divalent metal cations on mesoporous silicate MCM-41,Chem. Eng. J., 157 (2010) 25–28.
[9] M.M. Liu, L.A. Hou, S.L. Yu, B.D. Xi, MCM-41 impregnated with A zeolite precursor: Synthesis, characterization and tetracycline antibiotics removal from aqueous solution, Chem. Eng. J., 223 (2013) 678–687.
[10] K.M. Parida, S.K. Dash, Adsorption of Cu^{2+} on spherical Fe-MCM-41 and its application for oxidation of adamantine, J. Hazard. Mater., 179 (2010) 642–649.
[11] D. Perez-Quintanilla, I. del Hierro, M. Fajardo, Preparation of 2-mercaptobenzothiazole-derivatized mesoporous silica and removal of Hg(II) from aqueous solution, J. Environ. Monit., 8 (2006) 214–222.
[12] M.M. Liu, B.D. Xi, L.A. Hou, Synthesis, characterization, and mercury adsorption properties of hybrid mesoporous aluminosilicate sieve prepared with flyash, Appl. Surf. Sci., 273 (2013) 706–716.
[13] M.B. Amanda, F.Y. Wang, T. Grant Glover, MCM-41 impregnated with active metal sites: Synthesis, characterization, and ammonia adsorption, J. Hazard. Mater., 25 (2010) 58–62.
[14] S.A. Idris, C.M. Davidson, C.M. Manamon, Large pore diameter MCM-41 and its application for lead removal from aqueous media, J. Hazard. Mater., 185 (2011) 898–904.
[15] A.L.P.F. Caroni, D. Lima, C.R.M., M.R. Pereira, Tetracycline adsorption on chitosan: A mechanistic description based on mass uptake and zeta potential measurements, Colloids Surf., B.100 (2012) 227–228.
[16] P.Q. Damián, S. Alfredo, D.H. Isabel, Preparation, characterization, and Zn^{2+} adsorption behavior of chemically modified MCM-41 with 5-mercapto-1-methyltetrazole, J. Colloid Interface Sci., 313 (2007) 551–562.
[17] K.J. Choi, S.G. Kim, S.H. Kim, Removal of tetracycline and sulfonamide classes of antibiotic compound by powdered activated carbon, Environ. Technol., 29 (2008) 333–342.

[18] X.B. Wang, X.F. Zhang, Y. Wang, Investigating the role of zeolite nanocrystal seeds in the synthesis of mesoporous catalysts with zeolite wall structure, Chem. Mater., 23 (2011) 4469–4479.
[19] F.K. Shieh, C.T. Hsiao, H.M. Kao, Size-adjustable annular ring-functionalized mesoporous silica as effective and selective adsorbents for heavy metal ions, RSC Adv. 3 (2013) 25686–25689.
[20] S. Nethaji, A. Sivasamy, Adsorptive removal of an acid dye by lignocellulosic waste biomass activated carbon: equilibrium and kinetic studies, Chemosphere, 82 (2011) 1367–1372.
[21] M.M. Liu, L.A. Hou, Q. Li, X.J. Hu, S.L. Yu, Heterogeneous degradation of tetracycline by magnetic Ag/AgCl/modified zeolite X - persulfate system under visible light, RSC Adv. 6 (2016), 35216–35227.
[22] B.K. Vu, O. Snisarenko, H.S. Lee, Adsorption of tetracycline on La-impregnated MCM-41 materials, Environ. Technol., 31 (2010) 233–241.
[23] C. Gu, K.G. Karthikeyan, Interaction of tetracycline with aluminum and iron hydrous oxides, Environ. Sci. Technol., 39 (2005) 2660–2667.
[24] Y.P. Zhao, X.Y. Gu, S.X. Gao, Adsorption of tetracycline (TC) onto montmorillonite: Cations and humic acid effects, Geoderma, 183 (2012) 12–18.
[25] L. Zhang, X. Yan. S, X. Yan L. Studies on the removal of tetracycline by multi-walled carbon nanotubes, Chem. Eng. J., 178 (2011) 26–33.
[26] Z. Qing, Z.Q. Li, C.D. Shuang, Efficient removal of tetracycline by reusable magnetic microspheres with a high surface area, Chem. Eng. J., 210 (2012) 350–356.
[27] Y. Gao, Y. Li, L. Zhang, H. Huang, Adsorption and removal of tetracycline antibiotics from aqueous solution by graphene oxide, J. Colloid Interface Sci., 368 (2012) 540–546.
[28] Z. Li, P.H. Chang, J.S. Jean, W.T. Jiang, Interaction between tetracycline and smectite in aqueous solution, J. Colloid Interface Sci., 341 (2010) 311.
[29] M. Ersan, E. Bagda, E. Bagda, Investigation of kinetic and thermodynamic characteristics of removal of tetracycline with sponge like, tannin based cryogels, Colloids Surf., B., 104 (2013) 75–82.
[30] L.N. Wang, M. Xia, M.M. Liu, Sorption of tetracycline on organo-montmorillonites, J. Hazard. Mater., 225 (2012) 28–35.